Combined Surface Hardening and Laser Patterning Approach for Functionalising Stainless Steel Surfaces

Garcia Giron, Antonio; Romano, Jean-Michel; Liang, Yana; Dashtbozorg, Behnam; Dong, Hanshan; Penchev, Pavel; Dimov, Stefan

DOI:
10.1016/j.apsusc.2018.01.012

Document Version
Peer reviewed version

Citation for published version (Harvard):
Garcia Giron, A, Romano, J-M, Liang, Y, Dashtbozorg, B, Dong, H, Penchev, P & Dimov, S 2018, 'Combined Surface Hardening and Laser Patterning Approach for Functionalising Stainless Steel Surfaces', *Applied Surface Science*, pp. 516-524. https://doi.org/10.1016/j.apsusc.2018.01.012

Combined Surface Hardening and Laser Patterning Approach for Functionalising Stainless Steel Surfaces

A. GARCIA-GIRON[1,*], J. M. ROMANO[1], Y. LIANG[2], B. DASHTBOZORG[2], H. DONG[2], P. PENCHEV[1] AND S.S. DIMOV[1]

[1]*Department of Mechanical Engineering, School of Engineering, University of Birmingham, Edgbaston, Birmingham, B15 2TT, UK*

[2]*School of Metallurgy and Materials, University of Birmingham, Edgbaston, Birmingham, B15 2SF, UK*

*Corresponding author: Tel: +44 (0) 7843 859099; E-mail: a.garciagiron@bham.ac.uk

Abstract

The paper reports a laser patterning method for producing surfaces with dual scale topographies on ferritic stainless steel plates that are hardened by low temperature plasma surface alloying. Nitrogen and carbon based gasses were used in the alloying process to obtain surface layers with an increased hardness from 172 HV to 1001 HV and 305 HV, respectively. Then, a nanosecond infrared laser was used to pattern the plasma treated surfaces and thus to obtain super-hydrophobicity, by creating cell- or channel-like surface structures. The combined surface hardening and laser patterning approach allowed super-hydrophobic surfaces to be produced on both nitrided and carburised stainless steel plates with effective contact angles higher than 150^0. The hardened layers on nitrided samples had cracks and was delaminated after the laser patterning while on plasma carburised samples remained intact. The results showed that by applying the proposed combined approach it is possible to retain the higher hardness of the nitrided stainless steel plates and at the same time to functionalise them to obtain super-hydrophobic properties.

Keywords: Laser patterning; nanosecond laser; hydrophobicity; plasma surface alloying; hardening; surface engineering.

1. Introduction

Surface functionalisation technologies have many industrial applications due to the added value that they offer to existing and new emerging products. Especially, these technologies allow the surface properties of products to be modified, i.e. to enhance or incorporate new properties such as hydrophobicity [1], bacteria repellence [2], self-cleaning [3], heat transfer improvements [4], wear resistance [5] and/or anti-icing [6]. In markets with many competing products, customers are more likely to choose those that offer a better performance and integrate more functions while are still produced cost-effectively and hence are competitively priced. Therefore, the technologies for surface functionalisation are of great importance in many industrial sectors, e.g. in life sciences, transport, energy and other application areas. The two main approaches to obtain such functionalities involve

the use of either chemical treatments or require the surface compositions and topographies to be modified.

The surfaces can be classified depending on their wetting behaviour, in particular water droplets can be used to judge whether a given surface is hydrophilic (the drops spread) or hydrophobic (the drop stay rounded) [7]. To measure the surfaces' wetting properties, different techniques can be used, i.e. rolling angle, drop bouncing and static contact angle (CA). The latter is the easiest and quickest way to assess the wetting behaviour. When the static contact angle is lower than 90^0, the surface is considered hydrophilic while if it is higher - hydrophobic. Furthermore, when CA is higher than 150^0 the surface is considered super-hydrophobic[8,9]. Hydrophobic properties are often related to other phenomena, like self-cleaning [10] or anti-icing [11], that are of significant industrial interest. CA depends on the chemical compositions of liquids and surfaces that are in contact and also on surface topography/roughness [12–14]. The chemical compositions affect directly the surface energy of the three phases in contact, i.e. liquid, solid and air, and water droplets always take a shape that minimise it. At the same time, the contact angle between liquids and solids is affected by the surface roughness. If the roughness is sufficiently high air trapping between the liquid and the solid can occur that results in super-hydrophobic properties [15]. This is known as Cassie-Baxter state where topographies act as small air pockets to decrease the contact area between solids and liquids and thus lead to super-hydrophobicity. The effective CA when air is trapped between the drop and the solid can be calculated using Cassie-Baxter equation:

$$\cos\theta_{Cassie-Baxter} = \varphi\frac{\sigma_{SV}-\sigma_{SL}}{\sigma_{LV}} - (1-\varphi) \quad \text{Eq.1}$$

where: φ is the area fraction of the water-solid area to the projected area between a drop and a surface; and σ_{ij} - the surface tensions between the three interfaces, where ij are liquid-vapour (LV), solid-liquid (SL) or solid-vapour (SV) interfaces.

Processes employing chemical interactions with the substrate, such as chemical etching [16] or surface coatings [17], are widely applied by industry to obtain the desired surface properties. However, the use of chemical compounds results in wastes that are not environmentally friendly and require post processing to eliminate or manage them. Additionally, the chemicals can be applied only in special working areas as they can be hazardous to the workers.

While coatings are essentially applied to modify the surface tension, the wetting properties can be also changed by increasing the effective surface roughness, as shown in Eq.1. To engineer such micro topographies on surfaces and thus to improve their wetting behaviour, several technologies have been used successfully, e.g. photolithography [18], vertically aligned carbon nanotubes [19], electron-beam lithography [20], etc. However, these are multi-step complex processes that are usually difficult to scale up cost effectively to meet the requirements of many applications. Therefore, laser processing of surfaces has attracted a significant industrial interest as it offers a cost effective alternative in terms of efficiency and flexibility.

Also, hybrid processes were developed where both laser patterning and chemical etching were utilised. First, lasers were used to modify the roughness and then organic compounds were applied to change the surface energy and thus to produce surfaces with hydrophobic properties [21–24].

Ultra-short pulsed lasers were utilised to create patterns on various metallic surfaces and thus to change their wetting behaviours without the use of any chemical processes or coatings. Hydrophobicity was successfully obtained on different metals, such as stainless steel [25], titanium alloys [26], aluminium [27], copper [28] or nickel [29] through direct laser patterning with pico- and femto-second lasers.

The long processing times and high investment associated with the use of ultra-short lasers are a major limiting factor for the take up of this technology by industry. Therefore, near infrared (NIR) nanosecond lasers have attracted a significant interest as a cost-effective texturing route, especially to achieve relatively low processing time while the investment required is also low. The use of nano-second lasers to obtain hydrophobic surfaces on different metallic substrates has been reported, e.g. on aluminium alloys [30–32], stainless steel [33], copper and brass [34].

One of the major concerns when functionalising surfaces is their durability. If coatings are used due to wear or chemical interactions with surrounding environments the surface properties degrade and ultimately disappear over time. Consequently, the products' lifespans are reduced and also it may be necessary the coatings to be re-applied to recover the desired properties. The effect is similar on surfaces with functional topographies, where wear sand scratches modify them [35–37] and ultimately again the properties are lost over time. Thus, the use of hard, wear resistant materials is becoming an important prerequisite to increase the lifespan of functionalised surfaces.

Low temperature plasma surface alloying is a process used to increase surface hardness of metals [38]. Materials are hardened by diffusing atoms into surfaces to create interstitial supersaturated solid solutions that form thin layers of hardened material with up to 30 µm thickness. As the surfaces tend to expand while part's bulks are not affected, the hardened layers are stressed, in particular the surfaces are compressed and their hardness increases to up to 1500 HV. Low temperature plasma surface alloying has been successfully reported on several materials, e.g. Fe-Cr, Co-Cr [39]or Ni-Cr alloys [38], austenitic stainless steel [40], FeAl40 iron aluminide [41] or ferritic stainless steel [42]. Different gas mixtures are widely used during the treatment, and depending on their composition the interstitials on surfaces are C or N.

The research reported in this paper presents a laser patterning method for producing surfaces with dual scale topographies on ferritic stainless steel plates hardened by low temperature plasma surface alloying. In particular, a nanosecond laser is used to produce channels and cell-like surface structures on plasma treated surfaces and thus to obtain super-hydrophobic properties. The next section describes the experimental setup used in this research. Then, the results are presented and discussed and conclusions are made about the proposed approach that combines surface engineering with laser patterning to functionalise stainless steel surfaces.

2. Materials and Methods

2.1. Sample preparation

Ferritic stainless steel X6Cr17 plates with size of 50x50 mm and thickness of 0.7 mm were used in the experiments. The plates were grinded before the plasma treatments (1200 grit size) to remove surface contaminants and oxide layers. DC plasma carburising and nitriding processes were carried out in an adapted DC Klöckner Lonon 40 kVA plasma furnace. Any residual thin surface oxide films were removed by plasma sputtering to enable atomic diffusion into the surface. Samples were treated for 20 hours at 400°C in a gas pressure of 3 mbars and gas mixtures of 1.5% CH_4: 98.5% H_2 and 25% N_2: 75% H_2 for carburised and nitrided samples, respectively. Afterwards, all plates were cleaned in an ultrasonic bath with ethanol.

The depth of the treatment was determined using glow-discharge optical emission spectroscopy (GDOES) in Spectruma GDA 650HR analyser. Fig. 1 shows the chemical composition of the samples vs the depth after the plasma treatments. The depth of the hardened layer for the nitrided samples (25 µm) is higher than that obtained on the carburised ones (1 µm). Also, the mass concentration of

alloying elements on surfaces is 12.9% of C and 39.8% of N on carburised and nitrided samples, respectively.

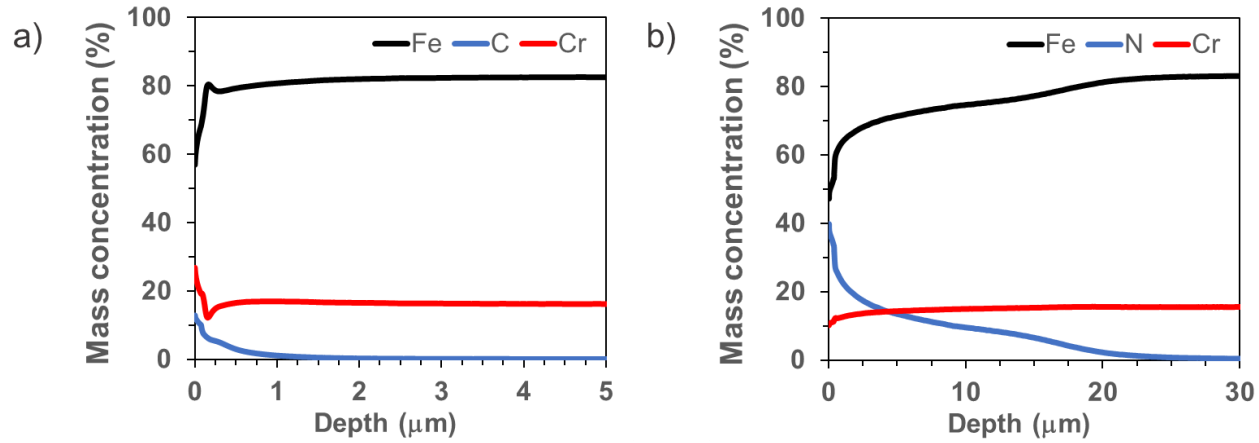

Fig 1. Mass concentration of the plasma carburised (a) and nitrided (b) samples vs the depth from the surface.

A Mitutoyo MVK-H1 micro-hardness tester fitted with a diamond Vicker's indenter and a load of 500 g was employed to measure the hardness of the surfaces before and after the plasma alloying process. The hardness of as-received ferritic stainless steel plates was 172 HV and 305 and 1001 HV for the carburised and nitrided samples, respectively.

The roughness was measured using an Alicona G5 focus variation microscope (x100 lens). The roughness of as-received stainless steel plates was Ra 49.4 nm and respectively 39.3 nm and 149.5 nm for the grinded carburised and nitrided plates.

2.2. Laser processing

The samples were patterned using a laser micromachining system. The system integrates a MOPA-based Yb-doped fibre nanosecond (ns) laser source (SPI G4 50W HS-S) with a maximum average power (P) of 50 W and wavelength of 1064 nm (λ), and 100 mm telecentric lens to achieve a beam spot diameter of 35 µm. The movements of the laser beam are CNC controlled and they are performed with a 3D scan head (RhoThor RTA) with maximum scanning speed of 2.5 m/s.

Two different pulse durations were used in the experiments, 15 and 220 ns, and laser parameters were adjusted to irradiate the processed surfaces with the same energy per line. The process setting for all samples produced with the two pulse lengths were as follows:

- 220 ns: a scanning speed of 150 mm/s, pulse frequency of 70 kHz and pulse energy of 50.14 µJ;
- 15 ns: a scanning speed of 132 mm/s, pulse frequency of 100 kHz and pulse energy of 30.89 µJ.

The energy per line, E, was calculated as follows:

$$E = \frac{E_p\, f}{S} = \frac{E_p}{PD} \qquad \text{Eq.2}$$

where: E_p is the pulse energy [µJ]; f - the pulse frequency; PD - the pulse distance [µm]; S - the scanning speed [mm/s]. By using Eq.2 E was maintained the same for both pulse durations, in particular 24.4 µJ/µm.

Two patterns were produced by changing the scanning strategies, in particular one with parallel lines/channels along the surface and the other with two intersecting lines at 90° to produce cell-like structures. The step over distance between two consecutive lines (hatch) was 100 µm for all samples.

All plates were cleaned with compressed air after the laser patterning to remove any debris. No chemicals or alcohols were used to avoid the contamination of the patterned areas with organics that can affect the surface energy and thus the wetting properties.

2.3. Characterization techniques

An Alicona G5 focus variation (FV) microscope was used to capture the 3D topographies of the produced patterns and thus to analyse the achieved ablation depths and also the volumes of redeposited material. Micrographs of the patterned surfaces together with their chemical compositions were obtained using a Hitachi TM 3030 Plus Scanning Electron microscope with an integrated Energy Dispersive X-Ray (EDX) spectrometer Quantax70. The wetting properties were analysed using a sessile drop technique employing an optical CA measurement system (Attension Biolin Scientific Theta T2000-Basic+) based in a liquid dispenser with an integrated camera. 6 µl drops of Milli-Q water were used in all measurements under ambient conditions. Static contact angles and rolling angles were measured.

Samples were cut and polished to mirror finish to perform hardness measurements at different depths from the processed surface. The measurements were performed on a NanoTest Vantage nano indenter (Micro Materials Ltd).

To test the abrasion resistance of the produced samples, a polisher device that integrates a Buehler Vector Power Head and a Buehler Phoenix Alpha grinder-polisher have been employed. Silicon carbide sandpapers, Buehler CarbiMet 600 (P1200), were used as an abrasive with an average grain diameter bigger than the patterns, in particular 15.3 µm, to study the samples' wear resistance. The rotation speeds of the grinder and the head were set at 150 rev/sec and 60 rev/sec respectively, while the load applied was 1.36 kg for 20 seconds and water was used to assist the process and remove the generated debris in the test. The samples were cut prior to the abrasion test in order to have the same surface area of 325 mm^2 and thus to apply the same pressure on all of them. The topographies of the patterns were captured before and after the tests by using an Alicona G5 Focus Variation Microscope, and the depth of the patterns was measured and the volume of the removed material was assessed, too.

3. Results and discussion

3.1. Ablation threshold

Prior to the laser patterning, ablation thresholds of as-received and the plasma treated plates were calculated using Liu's method [43]. The ablation thresholds were higher when the pulse duration of 220 ns was used in comparison with those obtained with 15 ns pulses as shown in Table 1. In addition, the ablation thresholds were higher after the plasma alloying both on carburised and nitrided plates.

Ablation thresholds (J/cm^2)

	220 ns	*15 ns*
Stainless steel	*3.98*	*2.23*
Nitrided	*5.25*	*2.38*
Carburised	*4.95*	*2.67*

Table 1. Ablation thresholds of as-received, carburised and nitrided samples obtained with pulse durations of 220 ns and 15 ns.

3.2. Microstructure analysis

Channels and cell-like structures were produced on as-received and plasma treated stainless steel plates by laser patterning, and their topographies were analysed employing a FV microscope. As the laser processing was carried out with pulses in the nano-second range, the ablation was followed by plasma expansion, ejection and re-deposition of molten material along the laser beam path. This led to the formation of dual scale patterns on surfaces, i.e. channels/cells produced by ablation and bulges around them resulting from the re-deposited molten material as shown in Fig 2. (a-b). Fig 2. (c) shows a cross section of the produced structures. As the step-over distance between the lines was the same during the laser patterning both with channels and cells, only two geometrical parameters were studied, the ablation depth (D) and the height of the solidified material (H). Multiple measurements on surfaces were taken to calculate the average values of H and D.

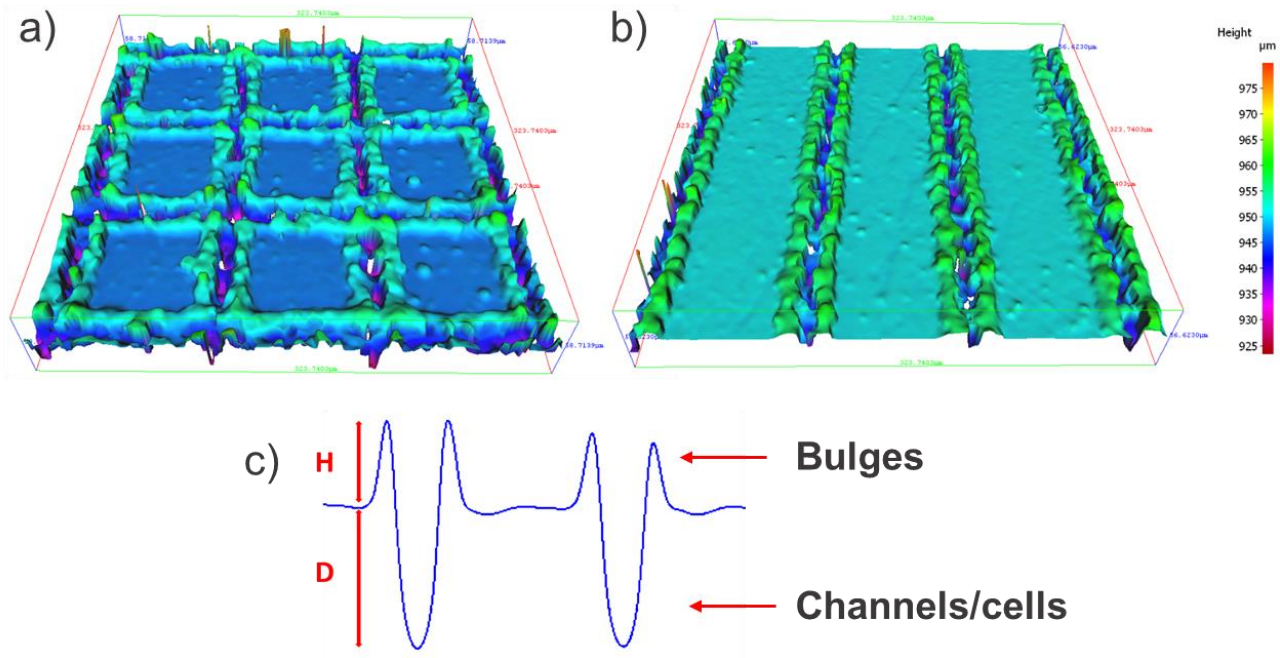

Fig 2. 3D topography of a cell-like pattern (a) and 3D topography of a channel like pattern (b), on an area of 323x323 µm; (c) cross-section of the 3D patterns, showing the height of redeposited material (H) and depth of ablation (D).

The D and H values obtained after laser patterning are given in Fig. 3. As can be seen the results obtained on as-received and plasma carburised samples are very similar, while those on the nitrided ones are different. The similarities between as-received and carburised samples can be attributed to the very small thickness of the hardened layer obtained with C, only 1 µm. As D of channels and cells are in the range from 4.07 to 8.83 µm, the hardened layer was removed with the first pulses and then the following pulses ablated the bulk of the stainless steel plates. In the case of the plasma nitrided samples, the thickness of the hardened layer is much higher, 25 µm, and therefore the bulk of the plates was not reached as D achieved with both pulse lengths were from 4.46 to 6.05 µm.

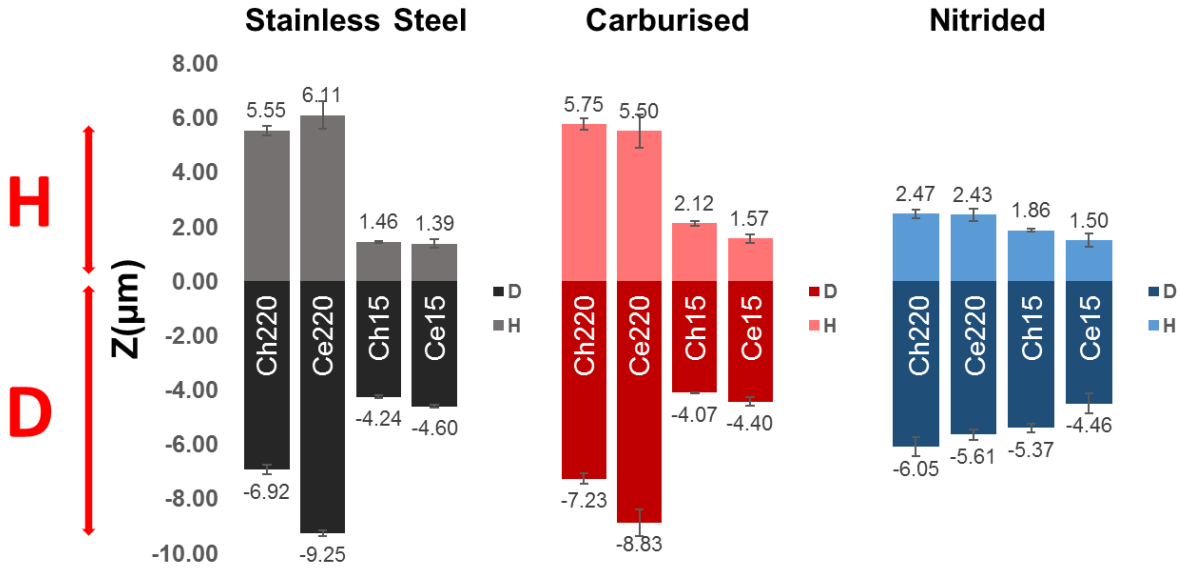

Fig 3. Ablation depths (D) and heights of bulges (H) for as-received and plasma treated samples.

Note: *Ch or Ce* denote samples with channels or cells, respectively, while *15 or 220* - the pulse length used for their patterning. For instance, the sample denoted as Ce220-Carburised would mean a cell-like pattern produced with a pulse length of 220 ns on a plasma carburised plate.

As can be expected the patterns produced with 220 ns pulses are deeper than those produced with 15 ns, due to the higher heat diffusion and subsequently the ejection and re-deposition of a bigger volume of molten material. Thus, the bulges resulting from the longer pulses are bigger and also the channels are deeper but the defences are less pronounced on nitride samples. On all samples the ablated volumes are in line with the ablation thresholds of as received and plasma treated stainless steel plates. In particular, the deeper patterns were produced with the longer pulses on the as-received and carburised plates as their ablation threshold were lower. Regarding the patterns produced with 15 ns pulses they had a similar depth as this is in line with the similar ablation thresholds of the three different types of plates investigated in this research.

The cell-like patterns are deeper than the channel-like ones on as-received and plasma carburised samples. In Fig. 3, the plotted depths for the cell-like patterns were measured along the lines only in order to compare the results with those obtained for the channel-like patterns. The depth at the intersections was measured, too and as expected it was almost twice higher, in particular the depths obtained with 220 and 15 ns pulses were 18.63 µm and 8.51 µm and 22.73 µm and 10.42 µm for as-received and plasma carburised samples, respectively. This can be explained with the twice high number of scans in the intersections and associated with the heat accumulation in producing the cell-

like patterns. However, this response was not observed on plasma nitrided samples, especially the depths obtained were 11.65 µm and 12.01 µm, respectively, and this could be explained with the recast formations that led to shallower and narrower channels and cells.

The SEM micrographs of the patterns produced on the three different types of plates investigated in this research are given in Fig. 4. In particular, one channel is shown or in the case of cell-like patterns the intersection between two lines is depicted where the effect of the heat accumulation is more pronounced. It can be observed that for all surfaces patterned with 220 ns pulses there is a higher volume of re-deposited material along the laser paths (see Fig. 3). In addition to the ejected material as a result of the plasma expansion, the dynamic effects of consecutive pulses reaching the surface contributed to the higher volume of re-deposited material. Especially, the trains of 220 ns pulses led to a higher agglomeration of solidified metal and also to the formation of thick and non-homogeneous structures with solidified drops on top. At the same time, when the patterning was performed with 15 ns pulses, the dynamic effects were much less pronounced and the resulting patterns were more homogeneous and uniform. Contrary to longer pulses, the effect of each 15 ns pulse can be seen and also the result of the overlap of consecutive pulses.

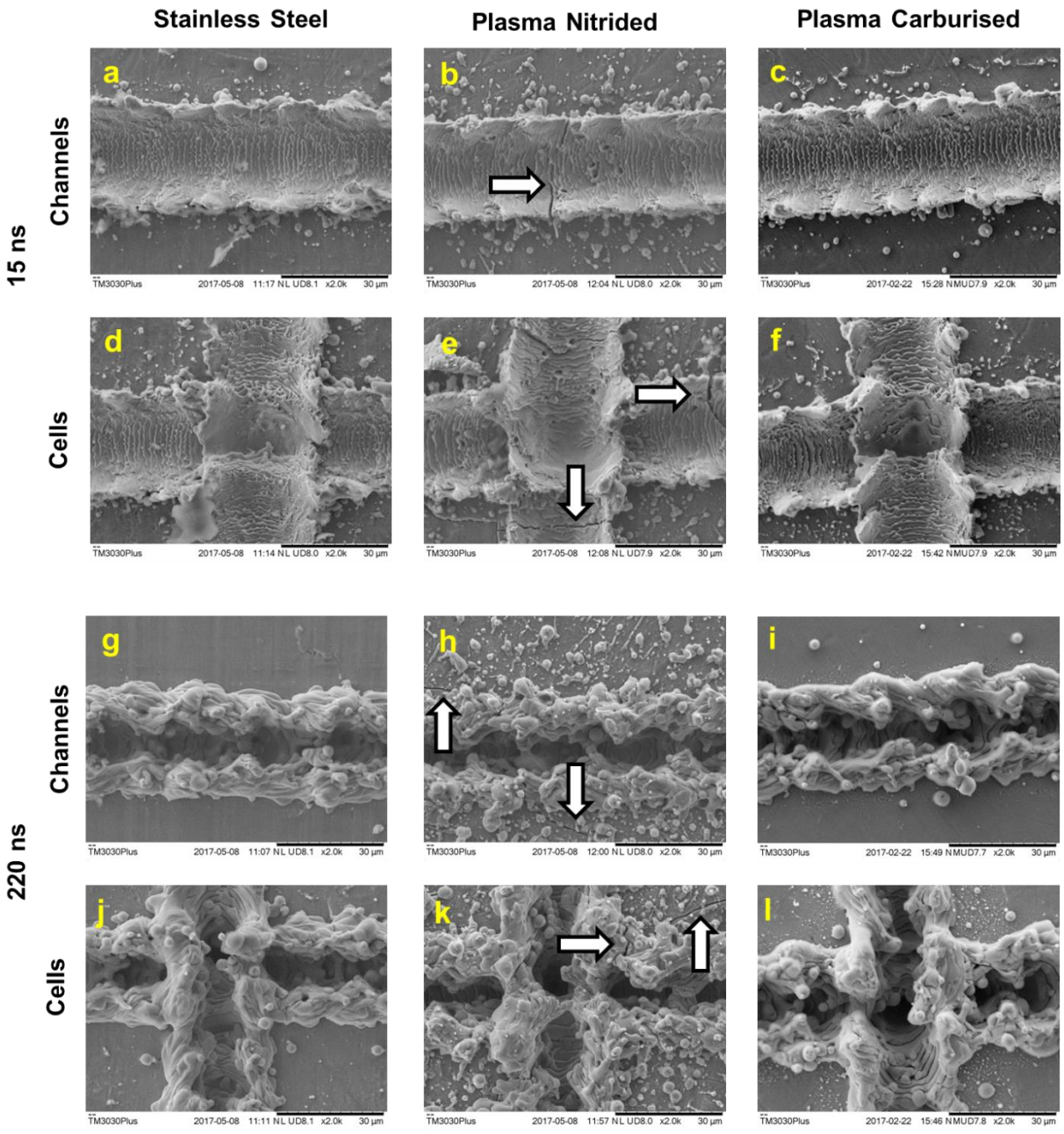

Fig 4. SEM micrographs of stainless steel and plasma treated samples patterned with 15 and 220 ns pulses. Cracks produced on the nitrided surfaces are pointed out with white arrows.

Surface quality obtained on plasma nitrided samples is slightly different, especially the splashes along the beam path are bigger and this is more pronounced when longer pulses were used. Also, cracks can be seen along the beam path and they are pointed out with arrows in Fig. 4. The presence of cracks can be explained with the plasma hardening and laser patterning mechanisms. As discussed above, during the plasma nitriding process a high concentration of the alloying element, N, is diffused in the material and leads to a hardness increase due to solid solution hardening mechanism. Then, when the surface is laser patterned, the highly nitrogen containing surface was abraded and the re-deposition material was radically solidified and/or self-quenched. As a consequence the re-deposited material becomes cracked in the surroundings of the processed area under the combined effects of the tensile stress caused by the rapid solidification and the brittle nature of quenched high-nitrogen steel. This is

supported by the observation that the appearance of cracks was observed only on plasma nitrided samples mainly due to the mass concentration of the alloying element, N.

3.3. Chemical analysis

Chemical compositions of the processed samples were analysed employing EDX spectrometry. The normalised elementary composition of the surfaces, calculated in weight, is shown in Table 2. The measurements were carried out on as-received and plasma treated samples after the laser patterning while the compositions of non-patterned surfaces were used as references.

	Stainless steel			Plasma carburised			Plasma nitrided		
	220 ns	15 ns	Ref	220 ns	15 ns	Ref	220 ns	15 ns	Ref
Fe	71.8	69.9	79.2	69.4	66.9	72.7	71.3	64.1	72.6
C	6.7	5.9	4.0	9.1	9.3	11.4	4.6	7.5	2.9
O	6.2	8.8	0.2	6.6	9.2	1.0	4.4	10.8	0.2
Cr	13.5	13.2	14.7	13.2	12.7	13.4	13.2	11.9	13.0
N	1.4	1.8	1.7	1.4	1.7	1.3	6.2	5.3	11.1
Mn	0.6	0.4	0.2	0.5	0.4	0.2	0.5	0.5	0.3

Table 2. Normalised chemical composition in weight (%) of stainless steel and plasma treated samples without (the reference one) and after laser patterning with 220 ns and 15 ns pulse durations.

As expected an increase of the alloying element was found after the plasma treatments, in particular the amount of carbon and nitrogen increased from 4.0% to 11.4% and from 1.7% to 11.1% on plasma carburised and nitrided samples, respectively. At the same time the amount of other elements remained the same and there were no traces of oxidation after the plasma treatment.

However, the oxygen content increased after laser patterning on all samples. This can be easily explained with the steel melting and solidification during the laser patterning that result in iron reacting with the oxygen present in air to form oxides along the beam path. The oxygen content was higher on the plates patterned with 15 ns pulses, most likely due to the higher patterns' depth achieved with 220 ns pulses that impeded the oxygen measurement at the bottom of the channels.

The amount of nitrogen detected on plasma nitrided samples was lower after the laser patterning and this can be attributed to the release of nitrogen in the processed area and/or some diffusion in the bulk due to the thermal load. On the contrary, the content of carbon on plasma carburised samples remained the same. This suggests a higher stability to thermal loads present in nanosecond laser patterning.

3.4. Wettability

Static CA measurements were performed to assess the wettability of the patterned surfaces with a droplet size of 6 µl. The wetting behaviour of the surfaces prior to laser patterning were measured,

too and the results were used as a reference. The measurement showed that they did not have super-hydrophobic properties, in particular CA of as-received, carburised and nitride surfaces were 78.9 ± 1º, 84.3 ± 6º and 101.4 ± 1º, respectively.

It is widely reported that laser patterned metallic surfaces show hydrophilicity just after the processing and with time CA increases until the surface is stabilized. The topographies remain the same and therefore any CA changes are attributed to surface chemistry, especially to the oxidation states of the processed surfaces [34] and the absorption of organic compounds from the air, due to the high porosity of the oxidised surfaces [25].

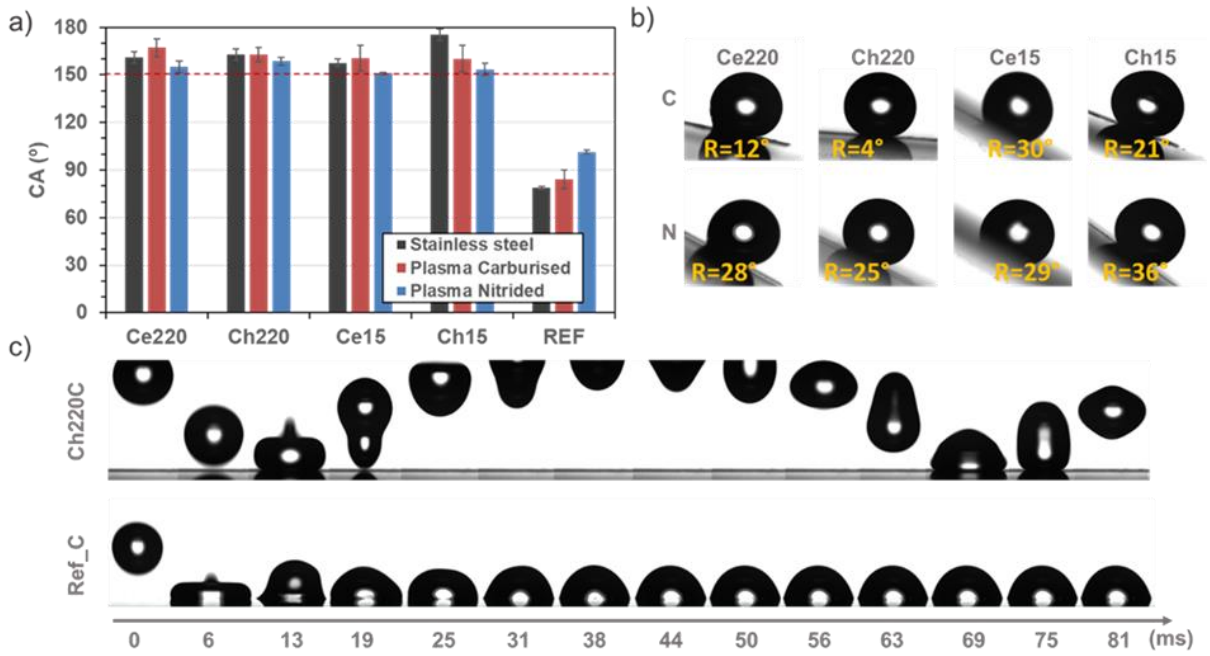

Fig 5. (a) Stabilized CA of laser patterned and reference surfaces. The dashed red line indicates the transition from hydrophobic to super-hydrophobic (CA higher than 150^o). (b) Sliding angles for the plasma carburised and nitrided samples after laser patterning. (c) Examples of water drops bouncing on plasma carburised stainless steel before (Ref_C) and after laser patterning.

All samples were highly hydrophilic just after the laser patterning. The water spread over the surface and therefore it was not possible to measure CA. Samples were analysed again after 10 days and then all of them were super-hydrophobic with CA higher than 150^0, as shown in Fig. 5 (a). As can be judged from the figure there was no significant difference in wetting behaviours of laser patterned as-received and plasma treated plates.

Drops on patterned areas did roll out when the samples were tilted, both on plasma nitrided and plasma carburised surfaces, as shown in Fig. 5 (b). Rolling angles were smaller for the samples patterned with 220 ns pulses, especially on the plasma carburised samples due to the patterns' higher aspect ratio. The impact of water drops was analysed, too, by employing a high speed camera at 160 frames per second. An example of a drop bouncing on a plasma carburised sample is provided in Fig.5 (c). It can be clearly seen in the figure that drops bounced several times only on the sample with the channel-like pattern.

Thus, it could be assumed that the Cassie Baxter state was achieved and water drops did not spread into the channels/cells. This phenomenon can be attributed to the hydrophilic iron oxides formed after the patterning that are porous and absorb organics from the air. Then, as a result, the patterned surfaces become non-polar [32] and in combination with the air pockets in the channels/cells they repel the water.

3.5. Hardness

The effects of heat dissipation on stability of the hardened layer were investigated. In particular, hardness measurements at different depths were performed with a nano-indenter on plasma treated surfaces after the laser patterning. After cutting the samples and polishing their cross section, the surface integrity was analysed with an optical microscope.

As it was already noted in Fig. 4, all nitrided surfaces were covered with cracks after the laser patterning, due to the high concentration of stresses on treated surfaces. This led to delamination of the nitrided layer and hence the loss of the surface properties. In the case of laser processing with shorter pulses (15 ns), the nitrided layer was significantly damaged after cutting the sample (see Fig. 6 (b)), while the layer was fully removed in the case of 220 ns pulses (see Fig. 6 (a)).

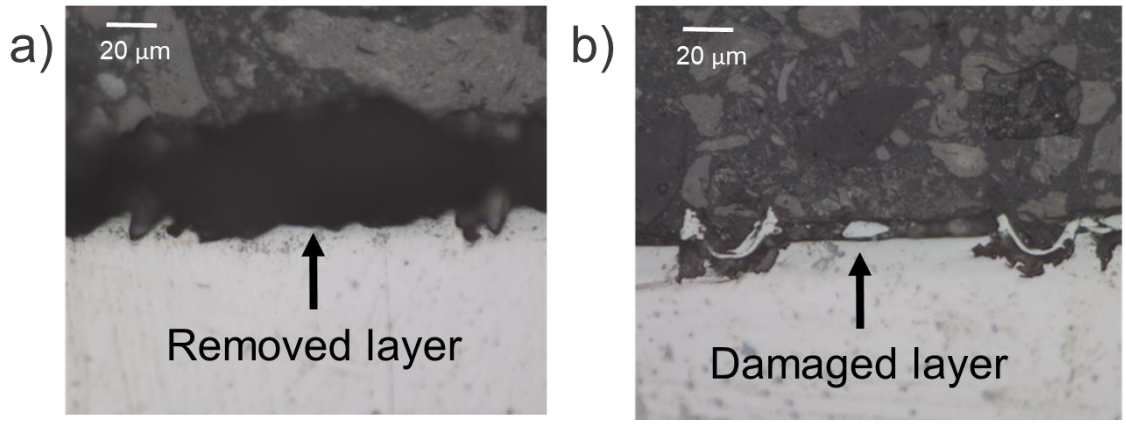

Fig 6. Cross-sections of the plasma nitrided samples after laser patterning with 220 ns (a) and 15 ns (b) pulses.

On the contrary, hardened layers on plasma carburised samples remained after laser patterning and there were no signs of any damage. Three different samples for each of the two considered pulse durations were analysed and typical micrographs of studied cross sections are given in Fig. 7. Channels produced with 220 ns and 15 ns pulse durations are shown in Fig. 7 (a) and Fig. 7 (b), respectively. The volume of redeposited material and the height of the bulges produced with the longer pulses were bigger. However, at the same time the hardness was similar and there were no other noticeable differences on the patterns produced with the two pulse durations considered in this research.

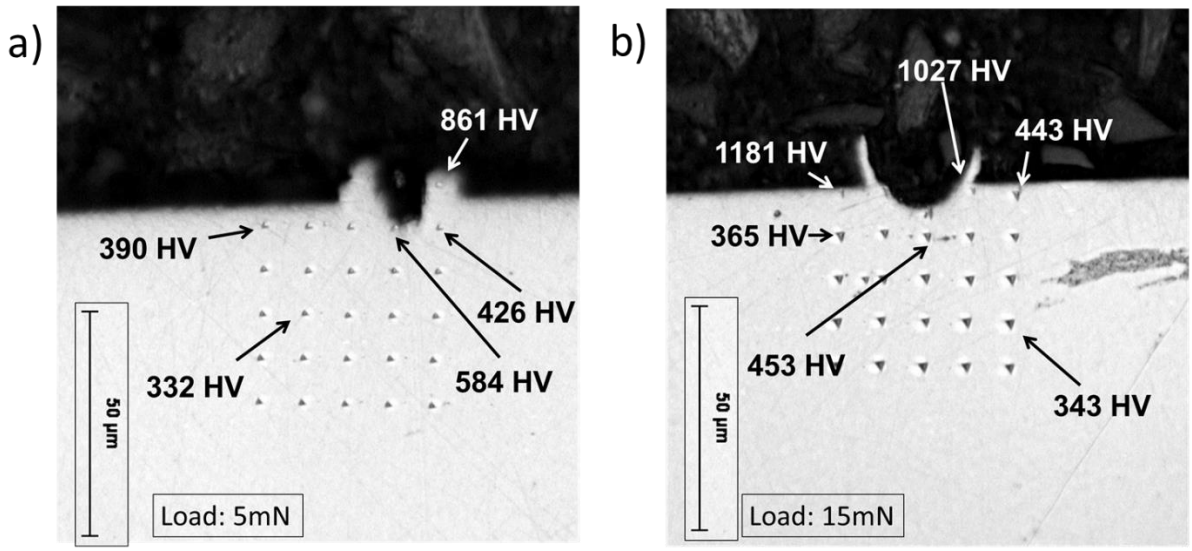

Fig 7. Cross sections of the channels produced with 220 ns (a) and 15 ns (b) pulse durations on plasma carburised samples with nano indentations at different depth from the processed surface.

The examination of both cross sections shows that the hardness close to the bottom of the channels is higher, approximately 600 HV, and it is gradually reduced to reach 300 HV away from the patterns that are the hardness values achieved after the plasma treatment.

The hardness of the bulges and their surroundings were also measured and the obtained values were higher than 800 HV as shown in Fig. 7 (a). This higher hardness can be explained by the thin carburised layer formed during the plasma treatment. It was also possible to measure the thin hardened layer on the patterns produced with the shorter pulses and values higher than 1100 HV was obtained, see Fig. 7 (b). This very high hardness value can be attributed to the thin carburised layer and the formation of martensite due to rapid self-cooling or quenching. The increased hardness of laser patterned areas can be explained with the heat dissipation into the bulk and the follow up self-cooling and quenching during the nanosecond laser-material interactions. At the same time should be stated that the heat affected zone is small and the thermal load does not modify the properties of the hardened layer.

3.6. Abrasion test

As discussed, the plasma nitrided surfaces had cracks after the laser patterning, and also the hardened layer delaminated. Therefore, the wear resistance of only as-received and plasma carburised samples were analysed and compared after channel-like patterning with the same pulse duration of 15 ns. In particular, both samples underwent the same abrasion tests, especially the same time and conditions were used, and also the topographies were analysed before and after the tests as shown in Fig. 8. It can be seen in the figure that in both cases the recasts were removed after the abrasion tests as they were mainly formed of brittle oxides. However, there was a significant difference in the depth of the channels, especially 41% and 18% reductions on as-received and plasma carburised samples, respectively, and hence there was a much higher loss of the patterns' depth on the as-received sample.

The static CA was measured after the abrasion tests, too, and they were 121.7 ± 1º and 138.5 ± 1º for the as-received and plasma carburised samples, respectively. This difference can be attributed to the smaller loss of channels' depth and also the remaining presence of carbon into the surface as the depth reduction after the abrasion test was smaller than the depth of the carbon diffusion shown in Fig. 1.

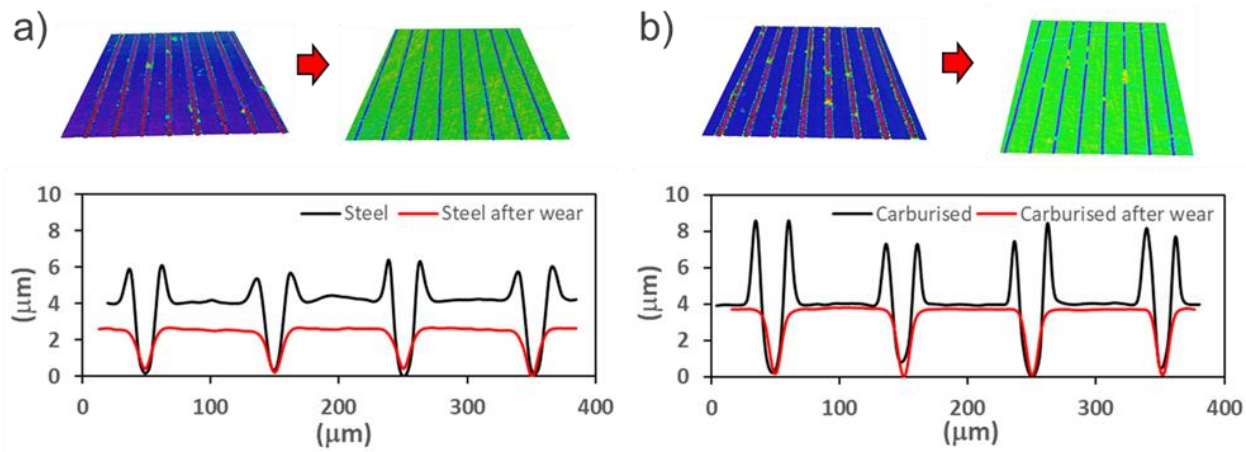

Fig 8. The topography and cross-sections of stainless steel (a) and plasma carburised (b) samples with channel-like patterns produced with 15 ns laser, before and after the abrasion test.

4. Conclusions

The combined effects of plasma surface alloying and nanosecond laser patterning on surface properties of stainless steel plates were studied in this paper. A laser patterning method was investigated for producing surfaces with dual scale topographies on ferritic stainless steel plates hardened by low temperature plasma surface alloying. The combined surface engineering and laser patterning approach allowed super-hydrophobic surfaces to be produced on both nitrided and carburised stainless steel plates with effective contact angles higher than 150^0. However, the nitrided samples exhibited cracks on the surfaces that led to delamination of the harden layer after the laser patterning. On the contrary, hardened layers on plasma carburised samples remained intact after the laser patterning. The results showed that by applying the proposed combined surface engineering - laser patterning approach it is possible to retain the higher hardness of the carburised stainless steel plates and at the same time to functionalise them and obtain super-hydrophobic properties. It was shown that the plasma carburised samples experienced much less wear compared with the as-received stainless steel substrates. Potentially, these combined effects can address one of the major concerns in functionalising stainless steel surfaces, in particular their resistance to wear and scratching. The future research will be focused on investigations of tribological properties such functionalised surfaces in the context of specific application in consumer products, automotive and tool making industries.

ACKNOWLEDGEMENTS

The research reported in this paper was carried out within the framework of European Commission H2020 ITN programme "European ESRs Network on Short Pulsed Laser Micro/Nanostructuring of

Surfaces for Improved Functional Applications" (www.laser4fun.eu) under the Marie Skłodowska-Curie grant agreement No. 675063. In addition, the work was supported by two other H2020 FoF programmes, i.e. the projects on "Modular laser based additive manufacturing platform for large scale industrial applications" (MAESTRO) and "High-Impact Injection Moulding Platform for mass-production of 3D and/or large micro-structured surfaces with Antimicrobial, Self-cleaning, Anti-scratch, Anti-squeak and Aesthetic functionalities" (HIMALAIA).

REFERENCES

[1] R. Wu, S. Liang, A. Pan, Z. Yuan, Y. Tang, X. Tan, D. Guan, Y. Yu, Fabrication of nano-structured super-hydrophobic film on aluminum by controllable immersing method, Appl. Surf. Sci. 258 (2012) 5933–5937. doi:10.1016/j.apsusc.2011.10.029.

[2] B. Laha, M. Ghosh, A. Chebolu, Nagahanumaiah, Investigation on bacterial adhesion and colonisation resistance over laser-machined micro patterned surfaces, Micro Nano Lett. 8 (2013) 280–283. doi:10.1049/mnl.2013.0109.

[3] R. Jagdheesh, M. Diaz, J.L. Ocaña, Bio inspired self-cleaning ultrahydrophobic aluminium surface by laser processing, RSC Adv. 6 (2016) 72933–72941. doi:10.1039/C6RA12236A.

[4] M. Zupančič, M. Može, P. Gregorčič, I. Golobič, Nanosecond laser texturing of uniformly and non-uniformly wettable micro structured metal surfaces for enhanced boiling heat transfer, Appl. Surf. Sci. 399 (2017) 480–490. doi:10.1016/j.apsusc.2016.12.120.

[5] K. Li, Z. Yao, Y. Hu, W. Gu, Friction and wear performance of laser peen textured surface under starved lubrication, Tribol. Int. 77 (2014) 97–105. doi:10.1016/j.triboint.2014.04.017.

[6] A.-M. Kietzig, M.N. Mirvakili, S. Kamal, P. Englezos, S.G. Hatzikiriakos, Nanopatterned Metallic Surfaces: Their Wettability and Impact on Ice Friction, J. Adhes. Sci. Technol. 25 (2011) 1293–1303. doi:10.1163/016942411X555872.

[7] J. Bico, U. Thiele, D. Quéré, Wetting of textured surfaces, Colloids Surfaces A Physicochem. Eng. Asp. 206 (2002) 41–46. doi:10.1016/S0927-7757(02)00061-4.

[8] K.M. Tanvir Ahmmed, A.-M. Kietzig, Drag reduction on laser-patterned hierarchical superhydrophobic surfaces, | Soft Matter Soft Matter. 12 (2016) 4912–4922. doi:10.1039/c6sm00436a.

[9] E. Bormashenko, Historical perspective Progress in understanding wetting transitions on rough surfaces, Adv. Colloid Interface Sci. 222 (2015) 92–103. doi:10.1016/j.cis.2014.02.009.

[10] G.S. Watson, D.W. Green, L. Schwarzkopf, X. Li, B.W. Cribb, S. Myhra, J.A. Watson, A gecko skin micro/nano structure - A low adhesion, superhydrophobic, anti-wetting, self-cleaning, biocompatible, antibacterial surface, Acta Biomater. 21 (2015) 109–122. doi:10.1016/j.actbio.2015.03.007.

[11] L. Mishchenko, B. Hatton, V. Bahadur, J.A. Taylor, T. Krupenkin, J. Aizenberg, Design of ice-free nanostructured surfaces based on repulsion of impacting water droplets, ACS Nano. 4 (2010) 7699–7707. doi:10.1021/nn102557p.

[12] J. Bico, C. Tordeux, D. Quéré, Rough wetting, Europhys. Lett. 55 (2001) 214–220. doi:10.1209/epl/i2001-00402-x.

[13] A. Malijevsky, Does surface roughness amplify wetting?, J. Chem. Phys. 141 (2014). doi:10.1063/1.4901128.

[14] A.T. Abdulhussein, G.K. Kannarpady, A.B. Wright, A. Ghosh, A.S. Biris, Current trend in fabrication of complex morphologically tunable superhydrophobic nano scale surfaces, Appl. Surf. Sci. 384 (2016) 311–332. doi:10.1016/j.apsusc.2016.04.186.

[15] B.H. Luo, P.W. Shum, Z.F. Zhou, K.Y. Li, Surface geometrical model modification and contact angle prediction for the laser patterned steel surface, Surf. Coatings Technol. 205 (2010) 2597–2604. doi:10.1016/j.surfcoat.2010.10.003.

[16] Y. Wu, Y. Wang, H. Liu, Y. Liu, L. Guo, D. Jia, J. Ouyang, Y. Zhou, The fabrication and hydrophobic property of micro-nano patterned surface on magnesium alloy using combined sparking sculpture and etching route, Appl. Surf. Sci. 389 (2016) 80–87. doi:10.1016/j.apsusc.2016.07.060.

[17] R.G. Joshi, A. Goel, V.M. Mannari, J.A. Finlay, M.E. Callow, J.A. Callow, Evaluating fouling-resistance and fouling-release performance of smart polyurethane surfaces: An outlook for efficient and environmentally benign marine coatings, J. Appl. Polym. Sci. 114 (2009) 3693–3703. doi:10.1002/app.30899.

[18] S. Suzuki, A. Nakajima, K. Tanaka, M. Sakai, A. Hashimoto, N. Yoshida, Y. Kameshima, K. Okada, Sliding behavior of water droplets on line-patterned hydrophobic surfaces, Appl. Surf. Sci. 254 (2008) 1797–1805. doi:10.1016/j.apsusc.2007.07.171.

[19] C. Lee, S. Baik, Vertically-aligned carbon nano-tube membrane filters with superhydrophobicity and superoleophilicity, Carbon. 48 (2010) 2192–2197. doi:10.1016/j.carbon.2010.02.020.

[20] X. Li, J. Shao, Y. Ding, H. Tian, Microbowl-arrayed surface generated by EBL of negative-tone SU-8 for highly adhesive hydrophobicity, Appl. Surf. Sci. 307 (2014) 365–371. doi:10.1016/j.apsusc.2014.04.039.

[21] H. He, N. Qu, Y. Zeng, Lotus-leaf-like microstructures on tungsten surface induced by one-step nanosecond laser irradiation, Surf. Coat. Technol. 307 (2016) 898–907. doi:10.1016/j.surfcoat.2016.10.033.

[22] A.M. Emelyanenko, F.M. Shagieva, A.G. Domantovsky, L.B. Boinovich, Nanosecond laser micro- and nanotexturing for the design of a superhydrophobic coating robust against long-term contact with water, cavitation, and abrasion, Appl. Surf. Sci. 332 (2015) 513–517. doi:10.1016/j.apsusc.2015.01.202.

[23] Y. Liu, J. Liu, S. Li, H. Zhiwu, S. Yu, L. Ren, Fabrication of biomimetic super-hydrophobic surface on aluminum alloy, J. Mater. Sci. 49 (2014) 1624–1629. doi:10.1007/s10853-013-7845-0.

[24] L.B. Boinovich, A.M. Emelyanenko, The behaviour of fluoro- and hydrocarbon surfactants used for fabrication of superhydrophobic coatings at solid/water interface, Colloids Surfaces A Physicochem. Eng. Asp. 481 (2015) 167–175. doi:10.1016/j.colsurfa.2015.05.003.

[25] P. Bizi-Bandoki, S. Valette, E. Audouard, S. Benayoun, Time dependency of the hydrophilicity and hydrophobicity of metallic alloys subjected to femtosecond laser irradiations, Appl. Surf. Sci. 273 (2013) 399–407. doi:10.1016/j.apsusc.2013.02.054.

[26] A.-M. Kietzig, S.G. Hatzikiriakos, P. Englezos, Patterned Superhydrophobic Metallic Surfaces, Langmuir. 25 (2009) 4821–4827. doi:10.1021/la8037582.

[27] J. Long, M. Zhong, H. Zhang, P. Fan, Superhydrophilicity to superhydrophobicity transition of picosecond laser microstructured aluminum in ambient air, J. Colloid Interface Sci. 441 (2015) 1–9. doi:10.1016/j.jcis.2014.11.015.

[28] J. Long, M. Zhong, P. Fan, D. Gong, H. Zhang, Wettability conversion of ultrafast laser structured copper surface, J. Laser Appl. 27 (2015) S29107. doi:10.2351/1.4906477.

[29] Y. Zhang, G. Zou, L. Liu, Y. Zhao, Q. Liang, A. Wu, Y.N. Zhou, Time-dependent wettability of nano-patterned surfaces fabricated by femtosecond laser with high efficiency, Appl. Surf. Sci. 389 (2016) 554–559. doi:10.1016/j.apsusc.2016.07.089.

[30] M.C. Sharp, A.P. Rosowski, P.W. French, Nanosecond laser texturing of aluminium for control of wettability, Proc. SPIE. 9657 (2015) 96570J. doi:10.1117/12.2179929.

[31] R. Jagdheesh, J.J. Garcia-Ballesteros, J.L. Ocaña, One-step fabrication of near superhydrophobic aluminum surface by nanosecond laser ablation, Appl. Surf. Sci. 374 (2016) 2–11. doi:10.1016/j.apsusc.2015.06.104.

[32] J.T. Cardoso, A. Garcia-Girón, J.M. Romano, D. Huerta-Murillo, R. Jagdheesh, M. Walker, S.S. Dimov, J.L. Ocaña, Influence of ambient conditions on the evolution of wettability properties of an IR-, ns-laser textured aluminium alloy, RSC Adv. 7 (2017) 39617–39627. doi:10.1039/C7RA07421B.

[33] V.D. Ta, A. Dunn, T.J. Wasley, J. Li, R.W. Kay, J. Stringer, P.J. Smith, E. Esenturk, C. Connaughton, J.D. Shephard, Laser textured superhydrophobic surfaces and their applications for homogeneous spot deposition, Appl. Surf. Sci. 365 (2016) 153–159. doi:10.1016/j.apsusc.2016.01.019.

[34] D. V. Ta, A. Dunn, T.J. Wasley, R.W. Kay, J. Stringer, P.J. Smith, C. Connaughton, J.D. Shephard, Nanosecond laser textured superhydrophobic metallic surfaces and their chemical sensing applications, Appl. Surf. Sci. 357 (2015) 248–254. doi:10.1016/j.apsusc.2015.09.027.

[35] S.P. Mishra, A.A. Polycarpou, Tribological studies of unpolished laser surface textures under starved lubrication conditions for use in air-conditioning and refrigeration compressors, Tribol. Int. 44 (2011) 1890–1901. doi:10.1016/j.triboint.2011.08.005.

[36] D. Bhaduri, A. Batal, S.S. Dimov, Z. Zhang, H. Dong, M. Fallqvist, R. M 'saoubi, On design and tribological behaviour of laser textured surfaces, Procedia CIRP. 60 (2017) 20–25. doi:10.1016/j.procir.2017.02.050.

[37] T. Ibatan, M.S. Uddin, M.A.K. Chowdhury, Recent development on surface texturing in enhancing tribological performance of bearing sliders, Surf. Coatings Technol. 272 (2015) 102–120. doi:10.1016/j.surfcoat.2015.04.017.

[38] H. Dong, S-phase surface engineering of Fe-Cr, Co-Cr and Ni-Cr alloys, Int. Mater. Rev. 55 (2010) 65–98. doi:10.1179/095066009X12572530170589.

[39] J. Chen, X.Y. Li, T. Bell, H. Dong, Improving the wear properties of Stellite 21 alloy by plasma surface alloying with carbon and nitrogen, Wear. 264 (2008) 157–165. doi:10.1016/j.wear.2006.12.012.

[40] S. Corujeira Gallo, H. Dong, Study of active screen plasma processing conditions for carburising and nitriding austenitic stainless steel, Surf. Coatings Technol. 203 (2009) 3669–3675. doi:10.1016/j.surfcoat.2009.05.045.

[41] Z. Zhang, X. Li, H. Dong, Plasma-nitriding and characterization of FeAl40 iron aluminide, Acta Mater. 86 (2015) 341–351. doi:10.1016/j.actamat.2014.11.044.

[42] B. Larisch, U. Brusky, H.-J. Spies, Plasma nitriding of stainless steels at low temperatures, Surf. Coatings Technol. 116–119 (1999) 205–211. doi:10.1016/S0257-8972(99)00084-5.

[43] J.M. Liu, Simple technique for measurements of pulsed Gaussian-beam spot sizes, Opt. Lett. 7 (1982) 196. doi:10.1364/OL.7.000196.